Microgravity Science and Technology (2025) 37:3
https://doi.org/10.1007/s12217-024-10155-3

RESEARCH

Recordings on PIEZO1-Overexpressing Oocytes in Microgravity

Simon L. Wuest[1] · Geraldine Cerretti[1] · Jennifer Polzer[1] · Simon Gerig[2] · Christoph Zumbühl[3] · Christian Jost[3] · Lukas Rüfenacht[2] · Robert Eberli[2] · Barbara Krucker-Bösch[1] · Julia Traversari[4] · Melanie Horn[4] · Daniel Invernot Pérez[4] · Christina Giger-Lange[1] · Karin F. Rattenbacher-Kiser[1] · Fabian Ille[1] · Gerhard Székely[2] · Soeren S. Lienkamp[4] · Marcel Egli[1,5]

Received: 12 August 2024 / Accepted: 25 November 2024

Abstract
Exposure to acute and prolonged microgravity triggers numerous physiological adaptations. To date, the underlying molecular mechanisms are not well understood, and several pathways have been proposed. Among other candidates, specific ion channels are hypothesized to be gravity dependent, but it has not been possible to conclusively demonstrate gravity dependency of specific protein entities. Therefore, we developed a miniaturized two-electrode voltage clamp (TEVC) that allowed electrophysiological experiments on *Xenopus laevis* oocytes using the GraviTower Bremen Prototype (GTB-Pro). The GTB-Pro is capable of flying experiments on a vertical parabolic trajectory, providing microgravity for a few seconds. As an interesting first candidate, we examined whether the nonselective mechanosensitive ion channel PIEZO1 is gravity dependent. The results showed no difference between PIEZO1-overexpressing and control oocytes under acute microgravity conditions.

Keywords Xenopus laevis oocytes · PIEZO1 · Mechanosensitive Ion Channel · Electrophysiology · Microgravity · GraviTower Bremen Prototype

Introduction

Exposure to acute and prolonged microgravity, such as in human space flight, triggers numerous physiological adaptations (Blaber et al. 2010; Williams et al. 2009; Demontis et al. 2017; Clément 2007; Graf et al. 2024). To date, the underlying molecular mechanisms are not well understood, and several pathways have been proposed. Among other candidates, specific ion channels are hypothesized to be gravity dependent. Ion channels are a large family of transmembrane proteins, which allow rapid exchange of ions along the ion's electrochemical gradient. They play key roles in numerous physiological functions and diseases. With the introduction of the patch-clamping technique, it was discovered that the gating properties of specific ion channels could also be triggered solely by mechanical stress of the membrane (Sachs and Morris 1998). To date, multiple so-called mechanosensitive ion channels (MSCs), also termed stretch-activated ion channels, have been identified. Even though MSCs are involved in multiple physiological and pathological functions (Gu and Gu 2014), the physiological functions of many MSCs are still unknown (Anishkin et al. 2014; Arnadottir and Chalfie 2010). One reason for this could be that the conventional patch clamping method highly stresses the lipid membrane (Sachs 2010), which is thought to be relaxed under normal physiological conditions (Dai and Sheetz 1995).

✉ Simon L. Wuest
simon.wueest@hslu.ch

1 School of Engineering and Architecture, Institute of Medical Engineering, Space Biology Group, Lucerne University of Applied Sciences and Arts, Obermattweg 9, CH-6052 Hergiswil, Switzerland

2 School of Engineering and Architecture, Institute of Mechanical Engineering and Energy Technology, CC Mechanical Systems, Lucerne University of Applied Sciences and Arts, Horw, Switzerland

3 School of Engineering and Architecture, Institute of Electrical Engineering, Lucerne University of Applied Sciences and Arts, Horw, Switzerland

4 Faculty of Medicine, Institute of Anatomy and Zurich Kidney Center, University of Zurich, Zurich, Switzerland

5 Innovation Cluster Space and Aviation (UZH Space Hub), University of Zurich, National Center for Biomedical Research in Space, Dübendorf, Switzerland

Published online: 06 January 2025

Electrophysiological experiments under elevated or lower gravity conditions, also in single cells, suggest that some ion channels could also be gravity dependent (reviewed in (Kohn and Ritzmann 2017; Wuest et al. 2018)). However, it has not been possible to conclusively demonstrate gravity dependency of specific protein entities. Reasons for this include financial, technical, operational, and safety constraints attached to the use of current low-gravity platforms, making delicate micromanipulations in flight difficult (reviewed in (Wuest et al. 2018)). For example, we developed an adapted patch-clamp device that was optimized for electrophysiological recordings on *Xenopus laevis* oocytes during parabolic flights. However, the setup that was easy to handle and allowed exchanging oocytes in flight came at a cost of a reduced signal-to-noise ratio (Schaffhauser et al. 2011; Wuest et al. 2017). In this work, we developed a miniaturized two-electrode voltage clamp (TEVC) that allowed electrophysiological experiments inside the GraviTower Bremen Prototype (GTB-Pro) capsule on oocytes from the *Xenopus laevis*. The GTB-Pro is capable of flying experiments on a vertical parabolic trajectory, providing microgravity for a few seconds. TEVC is a well-established technique for whole-cell recordings on *Xenopus laevis* oocytes (Stühmer and Parekh 1995). It has a high signal-to-noise ratio and does not locally stress the membrane (compared to conventional patch clamping). We examined whether the MSC PIEZO1 is gravity dependent by using native and PIEZO1-overexpressing oocytes. The nonselective cation channel PIEZO1 (Gottlieb and Sachs 2012; Wang and Xiao 2018; Soattin et al. 2016) is an interesting first candidate, as it is thought to play major roles in mechanosensing (Coste et al. 2010; Rocio Servin-Vences et al. 2017; Zeng et al. 2018). It has been well preserved over evolution, and homologs were identified in many animals, plants, and primitive eukaryotes (reviewed in (Soattin et al. 2016)). In mammals, PIEZO1 expression has been described in the bladder, colon, kidney, lungs, and skin (Coste et al. 2010). It is thought to be involved in numerous physiological functions, including cell volume regulation, cell migration, homeostasis of epithelial tissues, neuronal axon guidance, vascular development, and blood pressure regulation (reviewed in (Wang and Xiao 2018)). PIEZO1 also plays key roles in several diseases, including autosomal recessive congenital lymphatic dysplasia and hereditary xerocytosis (also known as dehydrated stomatocytosis) (reviewed in (Alper 2017)).

Materials and Methods

Experiment Design

Oocytes were isolated from donor *Xenopus laevis* by ovariectomy (see below). On the same day, oocytes were then injected with 50 ng of mRNA coding the MSC PIEZO1. Control oocytes were injected with an equal volume (50 nl) of water only. All experiments were done after an incubation period of six days, which yielded a robust PIEZO1 expression.

Successful expression of PIEZO1 was verified with an established TEVC (see below) and the drug Yoda1, which is known to activate PIEZO1 (Syeda et al. 2015; Lacroix et al. 2018; Wang et al. 2018; Lin et al. 2022). To confirm PIEZO1 expression also with a second independent method, oocytes from five donor frogs were additionally sent for proteomic analysis (see below).

Microgravity experiments were conducted once the hardware and experiment protocol had been established. For these experiments, injected oocytes were shipped to the Center of Applied Space Technology and Microgravity (ZARM), located in Bremen, Germany.

Oocytes & mRNA

Oocytes were isolated by ovariectomy according to the approved protocol. Deep anesthesia of mature female *Xenopus laevis* frogs was achieved by immersion in 0.1% buffered tricaine methane sulfonate (Sigma, A5040). Upon loss of righting and withdrawal reflexes and injection of 25 mg/kg flunixin meglumine (Flunixine NEO Biokema, Swissmedic 56110), a 1–1.5-cm-long incision was made in the ventral paramedian abdominal wall and a portion of the ovary (1–2 cm^3) excised under aseptic conditions. Remaining ovarian tissue was repositioned in the abdominal cavity, and the abdominal wall and skin were sutured using absorbable suture material (Ethicon, Z310H) and single surgeon's knots. Subsequently, the harvested tissue was placed in ND96 without Ca^{2+}, and oocytes were defolliculated using two forceps. Then, the oocytes were washed for 15 min, rotating at 10 rpm in ND96 without Ca^{2+}. Follicular tissue was removed using collagenase type 1A (Sigma C2674, 1 mg/ml) and trypsin inhibitor (Sigma T2011, ca. 0.1 mg/ml), rotating at 10 rpm until follicular layers detached from the oocytes (approximately 1 h at 16°C). Afterwards, the oocytes were washed again, rotating for 15 min with ND96 without Ca^{2+}, then washed twice with Barth medium and transferred into petri dishes. Finally, healthy, stage V–VI oocytes were selected by visual inspection under a binocular microscope. Oocytes were maintained in Barth medium at 16°C, and the medium was exchanged daily.

A plasmid containing mouse PIEZO1 (mPiezo1-IRES-eGFP) was a gift from Ardem Patapoutian (Addgene plasmid #80925) (Coste et al. 2010). The plasmid was linearized with PsiI-v2 (New England Biolabs, R0744S) and transcribed using the mMESSAGE mMACHINE™ T7 ULTRA Transcription Kit (ThermoFisher Scientific,

AM1345), which also adds a polyA signal. After measuring the mRNA concentration, it was stored at −80°C until use.

Oocytes were injected with PIEZO1 mRNA right after isolation. Injection needles were prepared by pulling glass tubes (3.5″ Drummond #3–000–203-G/X), and the tips were subsequently broken off with forceps. The injection needles were filled bubble-free with paraffin oil prior mounting into the injector. Then, either mRNA or water was aspired. Oocytes were individually impaled and injected with 50 nl of pure water or 50 ng mRNA dissolved in water.

Proteomic analysis was done on oocytes from five donor frogs six days after injection. Oocytes were washed three times with phosphate-buffered saline (PBS) and snap frozen in liquid nitrogen. Mass spectrometry-based proteomic analysis was subsequently performed at the Functional Genomics Center Zurich (FGCZ), as described in the supplementary material.

ND96 without Ca^{2+}, which was used for oocyte isolation, contained 96 mM NaCl, 2 mM KCl, 1 mM $MgCl_2$, and 5 mM HEPES. pH was adjusted to 7.4 using Tris. Oocytes were maintained in modified Barth medium containing 88 mM NaCl, 1 mM KCl, 0.82 mM $MgSO_4$, 0.41 mM $CaCl_2$, 0.33 mM $Ca(NO_3)_2$, 2.4 mM $NaHCO_3$, and 10 mM HEPES. pH was adjusted to 7.4 using Tris. To avoid contamination, 5 mg/l doxycycline (Acros Organics, #446,060,050) and 5 mg/l gentamicine (BioChemica, A1492) were added as well. TEVC experiments were done with 100Na containing 100 mM NaCl, 1.8 mM $CaCl_2$, 1 mM $MgCl_2$, 2 mM KCl, and 10 mM HEPES. Again, pH was adjusted to 7.4 using Tris.

Two-Electrode Voltage Clamp (TEVC)

Expression of PIEZO1 was confirmed with an established TEVC (Stühmer and Parekh 1995) at the University of Zurich. In total 49 PIEZO1-injected oocytes and 48 control oocytes originating from four donor frogs were measured. In doing so, an oocyte was placed in the TEVC and impaled with two pulled glass pipettes (Hilgenberg, 1407420) filled with 3 M KCl. The oocyte was then voltage clamped at −30 mV (holding potential) and continuously perfused with 100Na. Then, the current–voltage relation was measured from −180 mV to + 120 mV (voltage pulses for 140 ms each, 20 mV increments). After a 15-second recovery period, the medium was switched to 100Na containing 30 µM Yoda1, a known PIEZO1 agonist (Syeda et al. 2015; Lacroix et al. 2018; Wang et al. 2018; Lin et al. 2022), for 3 min. Immediately afterwards, the current–voltage relation was measured again. The Yoda1-senstive current (delta between the two curves) was computed from the two measurements (Supplementary Figure S1).

"OoDrop" Hardware

For the microgravity experiments, first, a miniaturized TEVC was developed, which could be accommodated in the GTB-Pro's capsule. The final design was small enough that four identical units could be integrated. The modified TEVC could be roughly split into six subunits: the core "mechanical setup", "electronics and data acquisition", "medium supply", "waste medium collection", "oocyte visualization", and "control and data visualization". The GTB-Pro's capsule consisted of several horizontal boards with a diameter of 600 mm, onto which the subunits could be mounted (Fig. 1).

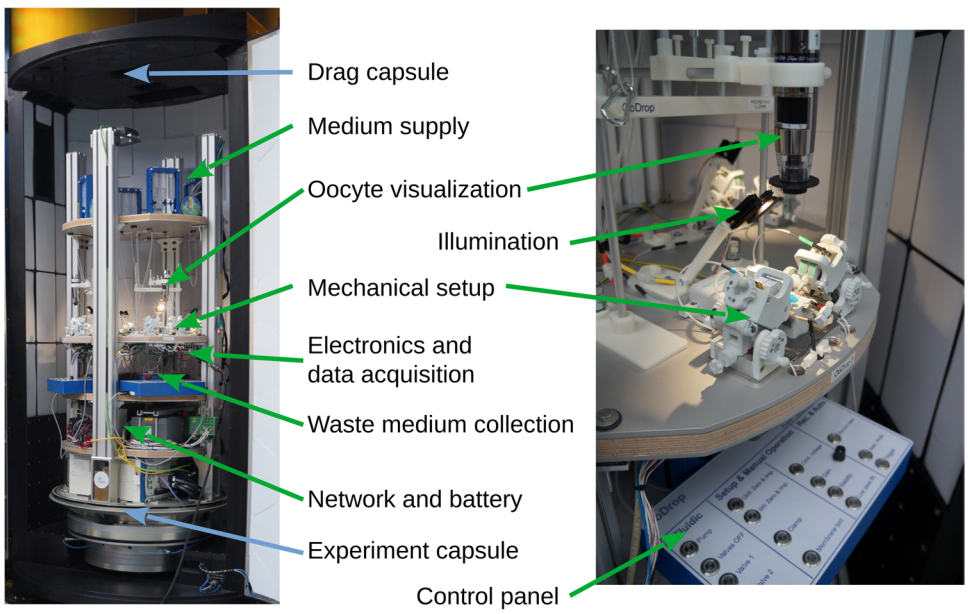

Fig. 1 Custom-made TEVC integrated in the GTB-Pro's capsule. The TEVC could be roughly split into the subunits: core "mechanical setup", "electronics and data acquisition", "medium supply", "waste medium collection", "oocyte visualization," and "control and data visualization" (not shown in figure). The subunits were attached to horizontal boards that were mounted on four vertical stringers. An additional "control panel" was used to facilitate setup of the voltage clamp

These horizontal boards were made of a sandwich structure of wood and aluminum on either side and attached to four vertical aluminum stringers. This structure effectively dampened possible vibrations or shocks during the experiment.

The main functions of the core "mechanical setup" (Fig. 2) were to precisely impale the oocyte with pulled glass pipettes to electrically access the cytosol and allow controlled perfusion of the oocyte. To avoid any movements of the glass pipettes due to changes in the gravitational load, a compact design with minimal lever length was chosen. KCl-filled glass pipettes (Hilgenberg, 1407420) were mounted in a narrow holder that included a silver-silver chloride (Ag/AgCl) pellet electrode (A-M Systems, 673443). The pipette was additionally secured with paraffin film before being mounted into the setup. The setup was mainly manufactured from 3D-printed PA12 using a HP Jet Fusion 580 Color. The base plate and a few selected parts were manufactured from aluminum or stainless steel to ensure mechanical stability. The setup allowed precise translation in three directions to position the glass pipette and impale the oocyte. Vertical translation was realized with an excentre, as the required range was small and the resulting design was very compact. Horizontal translation (back–forth) was realized with precision linear bearings with balls (Schneeberger, MINIRAIL 7), M4 plastic screws, and self-locking nuts, which were spring loaded to avoid mechanical overconstrains. Axial translation of the glass pipettes was completed with a similar design, also using linear bearings with balls (Schneeberger, MINIRAIL 5). The oocyte was positioned in a 3D-printed bath in which the bath electrodes (Ag/AgCl pellets) were integrated. The voltage-sensing bath electrode was mounted on the side, such that a KCl-soaked agarose bridge could be integrated between the electrode and the bath. Oocytes could be continuously perfused with up to three types of media. A simple, manually operated throttle allowed adjusting the flow velocity, and three valves allowed switching between media. Four setups were mounted in the GTB-Pro's capsule on a central board, such that they remained accessible to the experimenters.

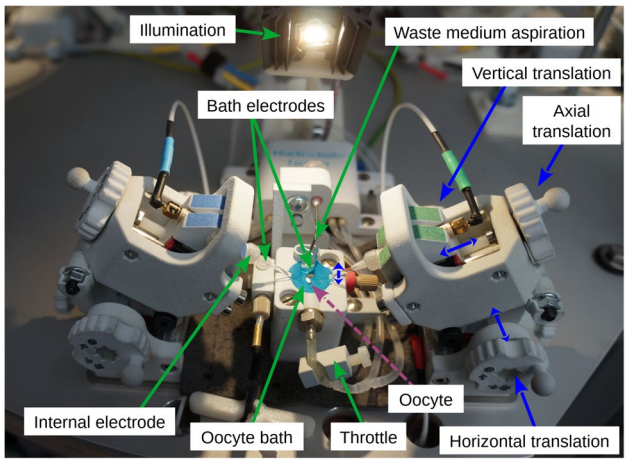

Fig. 2 The core "mechanical setup" allowed precise impalement of the oocytes with pulled glass pipettes and perfusion of the oocytes. Internal electrodes could be translated in a vertical, horizontal (back–forth), and axial direction to align the glass pipette and impale the oocyte. The oocyte was placed in a bath in which the bath electrodes were integrated. The voltage-sensing bath electrode was on the side, such that a KCl-soaked agarose bridge could be integrated. A throttle allowed adjustment of flow velocity, and waste medium was aspired by a needle. An LED illuminated the oocyte from the side to avoid disturbing reflections

Fresh medium was kept in three 50 ml-syringes (bBraun, 4617509F), which were installed on the top-level board to allow gravity-driven perfusion. The syringes were closed with a rubber cap (with a small hole for pressure equilibration) to avoid spills during GTB-Pro operation. Waste medium was aspired from the oocyte bath and collected on a board below the setup using four plastic beakers (Biosigma, BSC258) and a small eccentric diaphragm pump (Schwarzer Precision, 7s20099).

The "electronics and data acquisition" subunit was mounted on the lower side of the central board in a hanging configuration, such that the measuring wire's length remained minimal. It consisted essentially of a small data acquisition and control computer (NI, myRIO-1900) and a custom-made printed circuit board (PCB) with an integrated TEVC-circuit (Fig. 3). The signals were offset corrected, amplified, and low-pass filtered in analog. The voltage-clamp's proportional controller was realized on a field programmable gate array (FPGA), which was available on the myRIO devices. Whole-cell transmembrane current could be measured in two ranges, either ± 10 µA or ± 100 µA. Acquired data were low-pass filtered and down sampled on the myRIO device before being stored on a local SD card. Device control and data visualization were realized on a remote laptop via a network interface (TCP/IP). To set up the devices, impale the oocytes, and fine-tune the voltage-clamp, a separate control panel (Fig. 1) could be plugged into the PCB. This allowed the experimenters to execute the most frequent functions next to the setup using simple buttons. In this case, the remote laptop was only needed for data visualization. Oocytes were impaled under visual control. To avoid a binocular microscope, a digital USB microscope (Dino-Lite Edge, AM73115MTF) was used instead (Fig. 1). Illumination was ensured with an LED, which was mounted centrally from the oocyte bath (Fig. 2). Illumination from the side created less disturbing reflections than the LED ring of the digital microscope.

The four setups in the capsule were connected via a local network (TCP/IP) to a remote laptop. The network had an optical point-to-point bridge from the GTB-Pro's capsule to the ground segment, such that the experiment could still be controlled while the GTB-Pro was in operation. Continuous

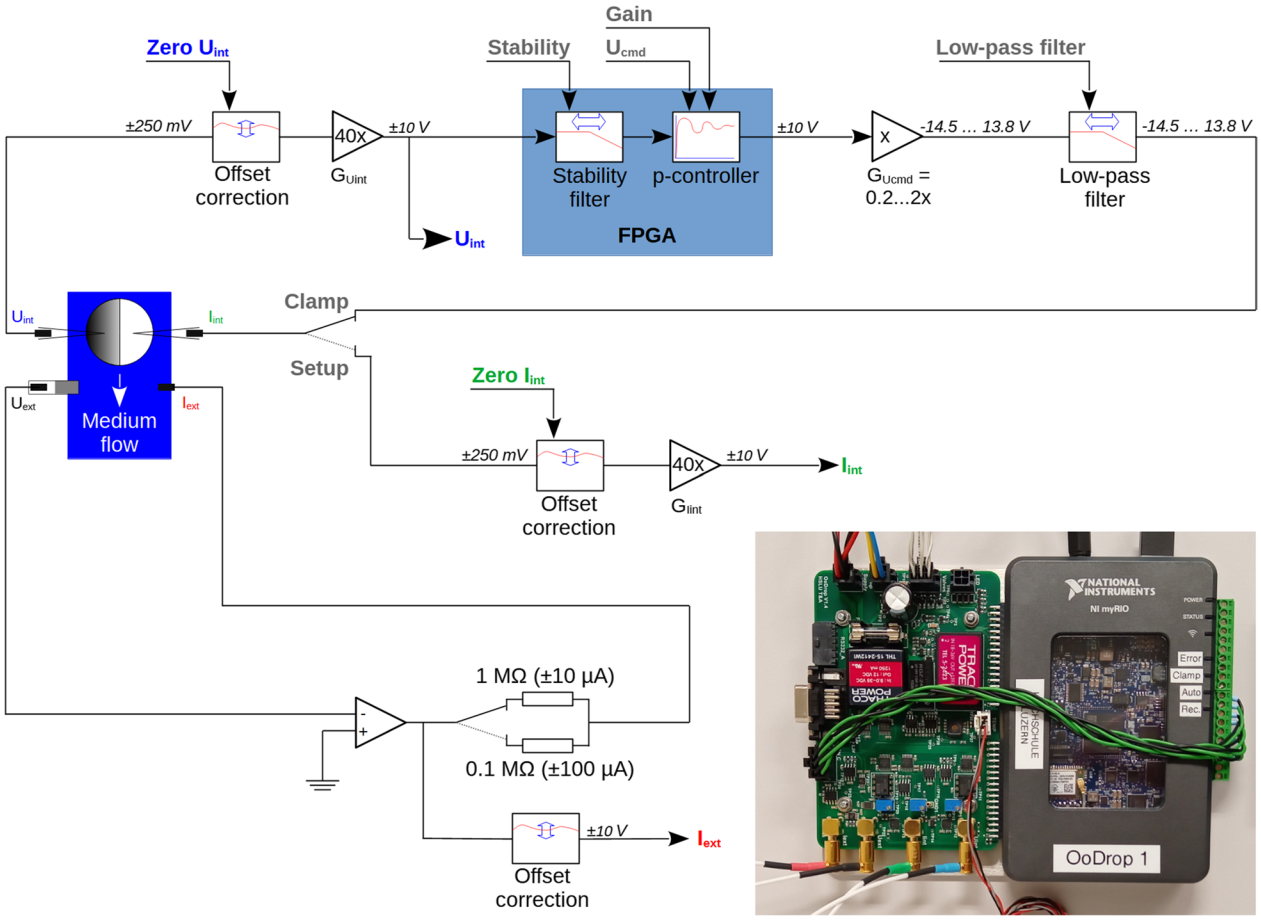

Fig. 3 TEVC electronics and data acquisition consisted of essentially of a data acquisition and control computer (NI, myRIO-1900) and a custom-made PCB with the integrated TEVC-circuit. The signals were offset corrected, amplified, and low-pass filtered in analog. The voltage-clamp's proportional controller was realized on a FPGA (available on myRIO). The transmembrane current was measured in the range of ± 10 µA or ± 100 µA (I_{ext}). U_{int} is the oocytes cytosolic voltage and U_{cmd} the desired command voltage. I_{int} was used to confirm successful penetration of the oocytes during setup. The voltage-sensing bath electrode (U_{ext}) was separated by a KCl-soaked agarose bridge from the bath

power was provided by a rechargeable battery. Network devices and the battery were installed in the lowest segment of the capsule (Fig. 1).

GraviTower Bremen Prototype (GTB-Pro)

Even though the GTB-Pro evolved from traditional drop towers, the underlying technology is very different (Könemann et al. 2015). This prototype's satisfactory performance made it appropriate for scientific use as of 2022 (Gierse et al. 2022). In short, the GTB-Pro consists of a closed drag-shield capsule driven by prestressed ropes and hydraulic engines along rails on a vertical parabolic trajectory (Gierse et al. 2017). Thus, the capsule is first accelerated upwards, then it goes into a controlled free-fall, and finally, the capsule is decelerated and brought to rest at its starting point. Acceleration and deceleration are experienced as hypergravity periods, while free-fall creates a microgravity condition. In contrast to other microgravity platforms, it provides the advantage that the parabolas' kinetics (dynamic acceleration and microgravity duration) can be chosen by the scientists within the limitations of the tower height (12 m) and engine power. This also allows soft initial accelerations for sensitive experiments and asymmetric parabolas. The GTB-Pro is designed to accommodate the same experiment capsules as used in the original Bremen drop tower (Dittus 1991; Kufner et al. 2011) to facilitate transition from one platform to the other. During the microgravity period, the experiment capsule inside the drag-shield capsule is released by a sophisticated release-and-catch mechanism. Thus, the experiment is actually free-flying and decoupled from disturbing external factors, such as air drag, rail friction, and eigenfrequencies from the drive system (Gierse et al. 2017).

Microgravity Experiments

For experiments under microgravity conditions, the protocol was adapted in comparison to the established reference TEVC to meet the constraints of the GTB-Pro. For the parabola, we chose an asymmetric kinetics with the smoothest possible acceleration before the microgravity period and harsh deceleration at the end. The initial acceleration was set to 1.5 g dynamically (2.5 g perceived) and final deceleration 3.4 g dynamically (4.4 g perceived). This yielded a microgravity period of approximately 1.8 s. To fit this short time, the current–voltage relation was adapted to series of 100-ms-voltage steps (−180, −20, −160, 0, −140, 20, −120, 40, −100, 60, −80, 80, −60, 100, −40, 120 mV), which were initiated just 50 ms after the gravity sensor detected microgravity.

The microgravity experiments were conducted six days after injection of PIEZO1 mRNA or water (control). Two oocytes were placed into two setups (as described above). After being impaled with the glass pipettes, the oocytes were voltage-clamped at −30 mV (holding potential) and perfused with 100Na. Ninety seconds before the parabola, perfusion was stopped, and 30 s later, the first current–voltage curve was recorded. After a one-minute recovery time, the GTB-Pro initiated the parabola (prestressing the ropes took ca. 15 s). The second current–voltage curve was recorded 50 ms after detection of microgravity. After a recovery time of 70 s, the third current–voltage relation was recorded again under normal gravity conditions. Finally, perfusion was restarted, and after 30 s, the medium was switched to 100Na containing 30 µM Yoda1 for 3 min. Subsequently, the last current–voltage relation was measured. While the switch to Yoda1 was still running, the capsule (suspended on an air bearing) was rotated carefully, and the next two oocytes were prepared, replacing the previously flown oocytes. PIEZO1-injected and control oocytes were approximately equally allocated among the setups to avoid a systematic bias caused by the hardware or the operators.

Data Analysis

Data of the microgravity experiments were acquired in a dedicated software program written in LabVIEW (2019). Data processing was partly done in LabVIEW and partly in MATLAB (R2022b). Data representation and statistical tests were performed using MATLAB.

To confirm expression of PIEZO1, the current–voltage relationship was computed (signal average over 100 ms) with and without application of Yoda1, a known agonist for the PIEZO1 channel (Syeda et al. 2015; Lacroix et al. 2018; Wang et al. 2018; Lin et al. 2022). Then, the Yoda1-senstive current was determined by computing the difference between the two readings (Supplementary Figure S1).

For the microgravity experiments, first, the current–voltage relationship was computed by averaging the current signal over 65 ms for each voltage step (the first 30 ms and the last 5 ms were ignored). Then, the difference between the recording before the parabola and in the parabola was computed to determine the microgravity effect. Similarly, the difference between the recording after the parabola and with the application of Yoda1 was computed to confirm PIEZO1 expression. Recordings in the GTB-Pro were more difficult than in the lab, and approximately half of the recordings had to be excluded. Oocytes were excluded from the analysis if one of the inclusion criteria in Table 1 were not met.

For statistical significance testing, the respective currents of all voltage steps were compared pairwise. For an easier presentation, the current–voltage curves were also reduced to the slope of a fitted line. Statistical significance was tested using the nonparametric Wilcoxon rank sum test. P-values below 5% were considered statistically significant.

Results

Starting five days after injection of 50 ng PIEZO1 mRNA, a Yoda1-sensitive current could be detected, which was absent in control oocytes. This current became robust six (Fig. 4) and seven days after injection. However, the quality of seven-day-old oocytes started to diminish drastically. Therefore, all following experiments were conducted six days after PIEZO1 injection. Proteomic analysis showed that PIEZO1 fragments could be found in PIEZO1-injected oocytes but not in the control oocytes in all five donor frogs.

We successfully miniaturized the TEVC such that four setups could fit into the GTB-Pro capsule (Fig. 1). Overall, the hardware performed sufficiently, but the procedure of impaling and voltage-clamping the oocytes was more difficult in the GTB-Pro than in the standard lab setup. About half of the oocytes failed during the recordings in the GTB-Pro, and the data had to be excluded. Under this aspect, easy access to the experiment and the high repetition rates of the GTB-Pro in comparison to traditional drop towers was very beneficial. Triggering the voltage protocol under the microgravity condition was reliable, and the measurements were always completed within the short microgravity period.

Table 1 For the microgravity experiments, oocytes were only included in the analysis if all of the inclusion criteria were met

Inclusion criteria	Value
Max. absolute current without Yoda1	≤ 4 µA
Max. absolute current with Yoda1	≤ 15 µA
Max. deviation from desired voltage	≤ 5 mV
Max. current instability (RMS)	≤ 1 µA

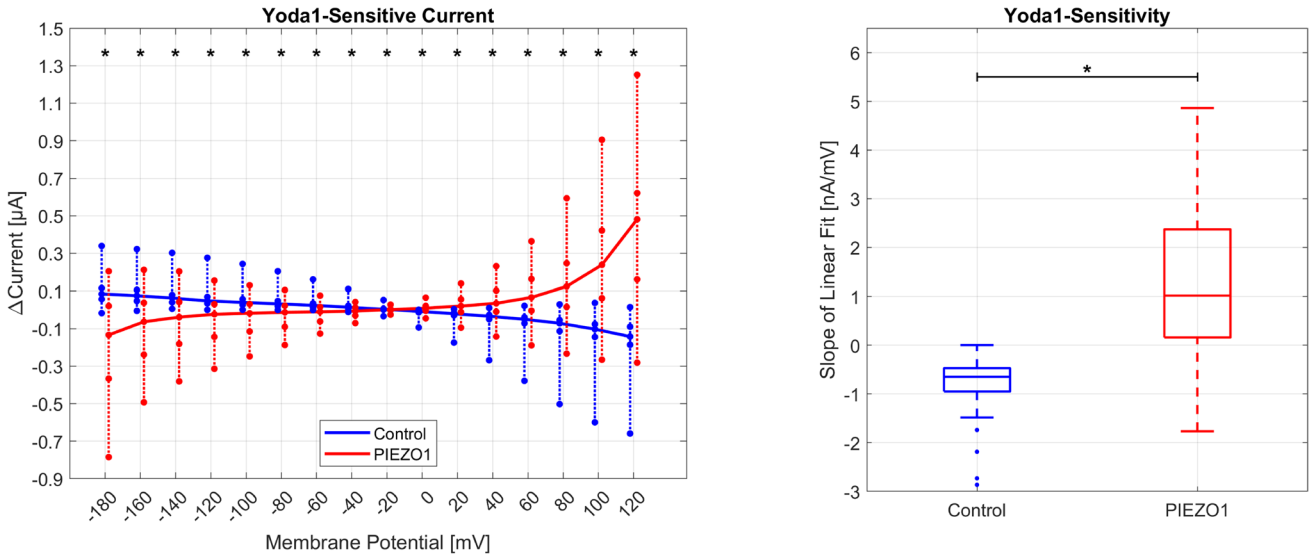

Fig. 4 Six days after injection of PIEZO1 mRNA, a Yoda1-sensitive current was detectable, which was absent in control oocytes. Left: Dots indicate the 0th, 25th, 75th, and 100th percentile of the current–voltage relation (delta current without and with the application of Yoda1). Medians are connected by a solid line. Right: Slope of a line fitted to the current–voltage relation. Boxplots indicate the 0th, 25th, 50th, 75th, and 100th percentile. Outliers are shown as individual points. The asterisk indicates statistical significance between control and PIEZO1-injected oocytes (Wilcoxon rank-sum test, $p < 5\%$)

(This was verified by a gravity sensor which was recorded simultaneously with the TEVC signals.) Even though the oocyte's bath remained open during the microgravity experiment, we did not observe any medium spillage. This agrees with GTB-Pro design and operation which generates only neglectable low magnitudes of negative gravity.

The experiments were done in two campaigns. In the first campaign, 32 control and 36 PIEZO1-injected oocytes originating from two donor frogs were included. The data showed no difference between PIEZO1-overexpressing and control oocytes under microgravity conditions (Fig. 5). The subsequent application of Yoda1 triggered a clear Yoda1-sensitive current, which was absent in control oocytes (Fig. 5). The current signal of the current–voltage relation was slightly smaller under microgravity (negative slope of the delta current, Fig. 5) for both groups. However, this difference is in the range of the difference seen between two consecutive measurements under standard lab conditions.

Based on the data from the first campaign, we were concerned that the difference between normal gravity and microgravity would not be sufficiently resolved. Therefore, we reduced the current measurement range (from ± 100 µA to ± 10 µA) to get a ten-fold resolution increase during the second campaign. Unfortunately, the oocytes from these two donor frogs were of lower quality, and voltage-clamping was especially difficult. Eleven control oocytes and eight PIEZO1-overexpressing oocytes were included. Of them, four control and six PIEZO1-overexpressing oocytes failed during the subsequent application of Yoda1. Therefore, no reliable statistical evaluation for this condition was possible. The data under microgravity condition confirmed that there was no difference between PIEZO1-overexpressing and control oocytes (Fig. 6).

Discussion and Conclusion

The application of Yoda1 in our setup and the reference TEVC triggered a Yoda1-senstitive current in PIEZO1 mRNA-injected oocytes but not in control oocytes six days after the injection. Yoda1 is known as an agonist of the PIEZO1 ion channel (Syeda et al. 2015; Lacroix et al. 2018; Wang et al. 2018; Lin et al. 2022). This demonstrated that the overexpression of PIEZO1 worked, which was also confirmed by proteomic analysis.

Conducting the experiment on the GTB-Pro with our miniaturized hardware was more demanding than experimenting under standard lab conditions, which is reflected in the high failure rate of the oocytes (ca. 50%). Compared to traditional microgravity platforms, the GTB-Pro provides easy access and a much higher repetition rate (Gierse et al. 2022). This allowed us to repeat the experiment often enough to compensate for the lost data. In total, 32 control and 36 PIEZO1-overexpressing oocytes were included in the first campaign. In the second campaign, with a finer resolution of the current signal, eleven control and eight PIEZO1-overexpressing oocytes could be included. None of the results from either campaign showed a difference

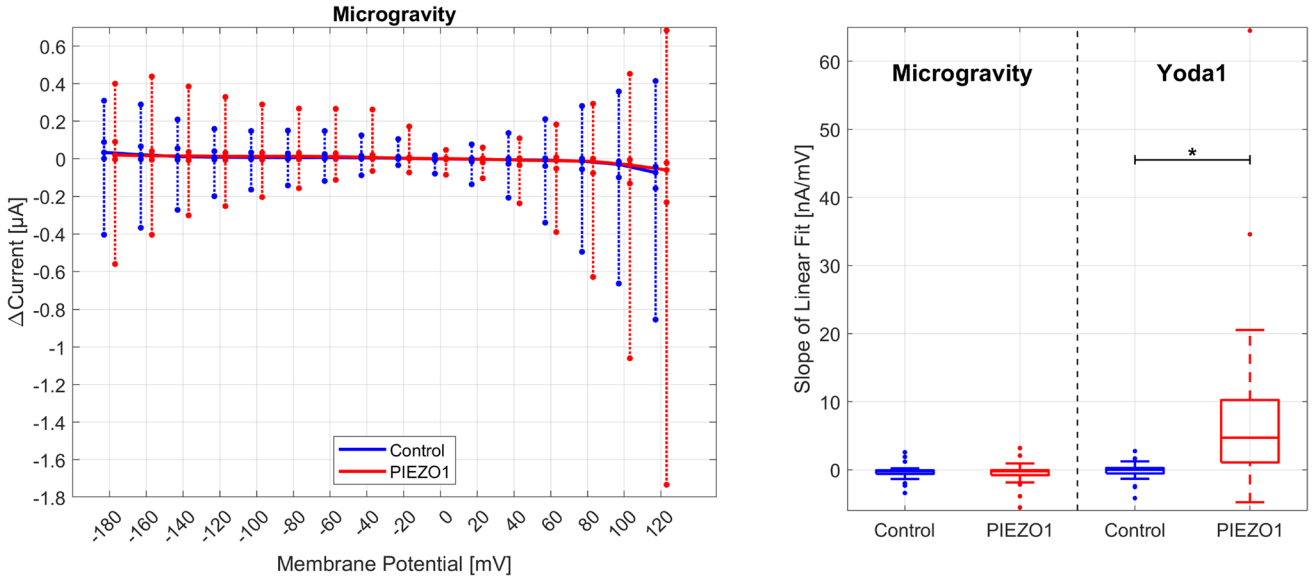

Fig. 5 Microgravity-dependent current acquired in the first experiment campaign with a course current range of ± 100 µA. The results were similar for PIEZO1-overexpressing and control oocytes. Left: Dots indicate the 0th, 25th, 75th, and 100th percentile of the current–voltage relation (delta current before the parabola and in microgravity). Medians are connected by a solid line. Right: Slope of a line fitted to the current–voltage relation. Boxplots indicate the 0th, 25th, 50th, 75th, and 100th percentile. Outliers are shown as individual points. The asterisk indicates statistical significance (Wilcoxon rank-sum test, $p < 5\%$). Yoda1 was applied after the parabola to confirm overexpression of PIEZO1

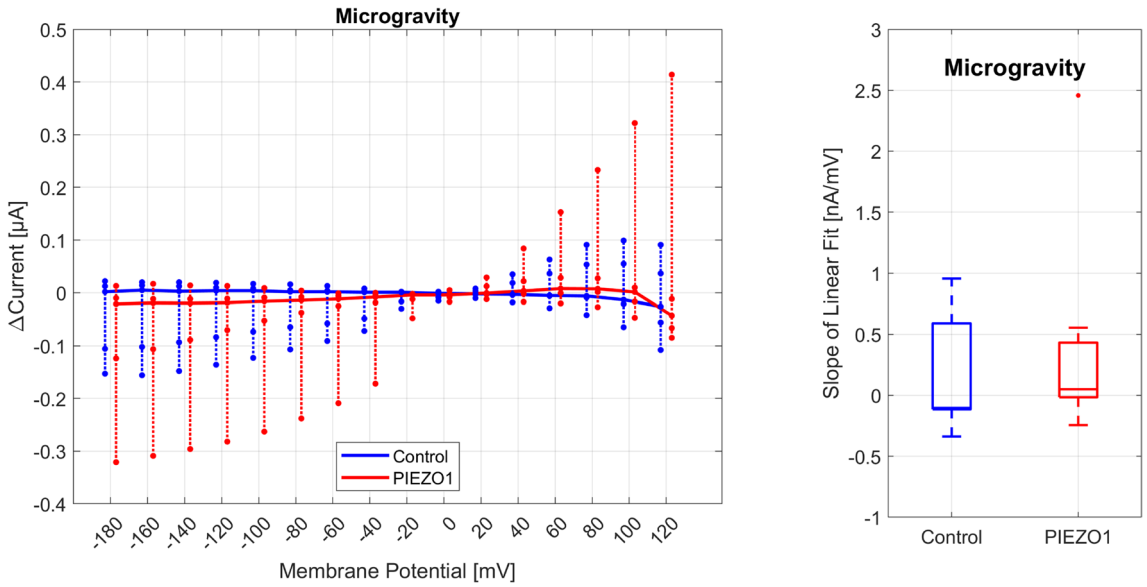

Fig. 6 Microgravity-dependent current acquired in the second experiment campaign with a fine current range of ± 10 µA. The results were similar for PIEZO1-overexpressing and control oocytes. Left: Dots indicate the 0th, 25th, 75th, and 100th percentile of the current–voltage relation (delta current before the parabola and in microgravity). Medians are connected by a solid line. Right: Slope of a line fitted to the current–voltage relation. Boxplots indicate the 0th, 25th, 50th, 75th, and 100th percentile. Outliers are shown as individual points. No statistical significance was detected (Wilcoxon rank-sum test, $p < 5\%$)

between control and PIEZO1-overexpressing oocytes (Fig. 5 and Fig. 6). Additionally, the small difference between normal gravity just before the parabola and microgravity was in the range of the difference seen between two consecutive readings under normal gravity conditions in the lab. The recordings right after the parabola suggest that the oocyte's membranes remained intact and that PIEZO1 remained sensitive to Yoda1.

This finding is partly in disagreement with previous experiments on *Xenopus laevis* oocytes during parabolic flights. A study that used an adapted TEVC on native oocytes showed a reduced current in the voltage-current relationship and a reduced current at −100 mV holding potential in microgravity (Richard et al. 2012). Another experiment that also used native oocytes and an adapted patch-clamp setup showed a tendency toward reduced Ca^{2+}-dependent current in response to a three-voltage step protocol under microgravity conditions (Wuest et al. 2017). An earlier study using a similar setup on an oocyte overexpressing the epithelial sodium channel (ENaC) showed a reduced conductance in microgravity and an increased conductance during elevated gravity (Schaffhauser et al. 2011). The reasons for these disagreements remain speculative at this point. First, the experiments cannot directly be compared due to the differences in setups, experiment protocol, sample numbers, and microgravity duration. Parabolic flights offer up to 22 s of microgravity time but come with significant limitations due to safety and organizational constraints (Wuest et al. 2018). Therefore, exchange of oocytes is limited, leading to low sample numbers. In this experiment, oocytes were replaced after each parabola, and oocytes from at least two donor frogs were used per campaign. This allowed more solid statistics and reduced the chance of coincidental findings due to biological variability. Furthermore, the less limiting safety constraints at the GTB-Pro facility allowed the sharp glass pipettes required for TEVCs with a high signal-to-noise ratio. However, these advantages came at a compromise of a much shorter microgravity period—only approximately 1.8 s in this experiment. Therefore, the recordings had to be executed very quickly.

Even though we did not observe an instantaneous change in basal PIEZO1 activity under microgravity conditions, microgravity could still act as a modulator of the gating properties in combination with other mechanical stimuli, such as shear stress, osmotic stress or pocking (Anishkin et al. 2014). However, in this initial study we refrained from adding a second mechanical stimulus in microgravity condition. Furthermore, recent publications demonstrated that PIEZO1 rapidly inactivates in response to a pocking stimulus and fully recovers only after around one minute (Lewis and Grandl 2020; Wijerathne et al. 2022). This could be a caveat of the short parabola, as an early inactivation of PIEZO1 channels could have masked a potential microgravity effect. Nevertheless, the acquired current signals between the onset of the parabola and until the first voltage step in microgravity, did show a systematic change that would suggest altered PIEZO1 activity.

In conclusion, we found no evidence (above the methodological sensitivity threshold) that would suggest altered basal activity of the mechanosensitive, nonselective cation channel PIEZO1 in response to short, acute microgravity. The data also suggest that the current–voltage relationship does not change instantaneously in response to short microgravity.

Mass Spectrometry based Proteomics Analysis

Sample Preparation

Proteomic analysis was done on oocytes from five donor frogs six days after injection. Oocytes were washed three times with phosphate-buffered saline (PBS) and snap frozen in liquid nitrogen. Mass spectrometry-based proteomics analysis was subsequently performed at the Functional Genomics Center Zurich (FGCZ). Samples were enriched for membrane fraction using a Mem-PER™ Plus Membrane Protein Extraction Kit (ThermoFisher Scientific, 89,842). Samples were then boiled in a final concentration of buffered 4% sodium dodecyl sulfate (SDS), pH 8.5 for 10 min at 95°C, followed by mechanical lysis using a tissue homogenizer (2 × 2-min cycles at 30 Hz, TissueLyser II, QUIAGEN) and high-intensity focused ultrasound (HIFU). Protein concentration was estimated using the Lunatic UV/Vis absorbance spectrometer (Unchained Lab), and a protein amount of 25 µg per sample was used. Subsequently, proteins were reduced and alkylated by adding Tris(2-carboxyethyl)phosphine and 2-Chloroacetamide to a final concentration of 5 mM and 15 mM, respectively. The samples were incubated for 30 min at 30°C, 700 rpm, and light protected. Samples were processed using the single-pot solid-phase enhanced sample preparation (SP3). The SP3 protein purification, digest, and peptide clean-up were performed using a KingFisher Flex System (Thermo Fisher Scientific) and carboxylate-modified magnetic particles (GE Life Sciences; GE65152105050250, GE45152105050250) (Hughes et al. 2014). Beads were conditioned following the manufacturer's instructions, consisting of three washes with water at a concentration of 1 µg/µl. Samples were diluted with 100% ethanol to a final concentration of 60% ethanol. The beads, wash solutions, and samples were loaded into 96 deep well- or micro-plates and transferred to the KingFisher. Following steps were carried out on the robot: collection of beads from the last wash, protein binding to beads, washing of beads in wash solutions 1–3 (80% ethanol), protein digestion (overnight at 37°C with a trypsin:protein ratio of 1:50 in 50 mM Triethylammoniumbicarbonat [TEAB]), and peptide elution from the magnetic beads using MilliQ water. The digest solution and water elution were combined, dried completely, and resolubilized in 20 µl of MS sample buffer (8% acetonitrile, 0.1% formic acid, 0.015% DDM) (n-dodecyl β-D-maltoside).

LC-MSMS

Liquid chromatography with tandem mass spectrometry (LC–MS/MS) analysis was performed on an Orbitrap Fusion Lumos (Thermo Scientific) equipped with a Digital PicoView source (New Objective) and coupled to an M-Class UPLC (Waters). The solvent composition of the two channels was 0.1% formic acid for channel A and 99.9% acetonitrile in 0.1% formic acid for channel B. The column temperature was 50°C. For each sample, 0.2 Abs of peptides (based on Lunatic output) were loaded on a commercial ACQUITY UPLC M-Class Symmetry C18 Trap Column (100 Å, 5 µm, 180 µm × 20 mm, Waters) connected to an ACQUITY UPLC M-Class HSS T3 Column (100 Å, 1.8 µm, 75 µm × 250 mm, Waters). The peptides were eluted at a flow rate of 300 nl/minute. After a 3-min initial hold at 8% B, a gradient from 8 to 32% B in 80 min and 32% to 42% B in additional 10 min was applied. The column was cleaned after the run by increasing to 95% B and holding 95% B for 10 min prior to reestablishing the loading condition.

The mass spectrometer was operated in data-dependent mode (DDA), prioritizing in-silico digested peptide precursors of PIZEO1 using an inclusion list, with a maximum cycle time of 3 s. Funnel RF level was at 40%, heated capillary temperature at 275°C, and advanced peak determination (APD) on. Full-scan MS spectra (300 − 1,500 m/z) were acquired at a resolution of 120,000 at 200 m/z after accumulation to an automated gain control (AGC) target value of 500,000 or for a maximum injection time of 40 ms. Precursors with an intensity above 5,000 were selected for MS/MS. Ions were isolated using a quadrupole mass filter with 1.6 m/z isolation window and fragmented by higher-energy collisional dissociation (HCD) using a normalized collision energy of 35%. Fragments were detected in the linear ion trap with the scan rate set to rapid, the automatic gain control set to 10,000 ions, and the maximum injection time set to 50 ms. Charge-state screening was enabled, and singly, unassigned charge states and charge states higher than seven were excluded. Precursor masses previously selected for MS/MS measurement were excluded from further selection for 20 s, applying a mass tolerance of 10 ppm. The samples were acquired using internal-lock mass calibration on m/z 371.1012 and 445.1200. The mass spectrometry proteomics data were handled using the local laboratory information management system (LIMS) (Türker et al. 2010).

Peptide Identification – Mascot – Scaffold

The acquired raw MS data were converted into Mascot generic format files (.mgf) using ProteoWizard (http://proteowizard.sourceforge.net/), and the proteins were identified using the Mascot search engine (Matrix Science, version 2.7.0.1). Spectra were searched against a Uniprot Mus Musculus proteome database (taxonomy 10,090, version from 20,220,503), concatenated to its reversed decoyed fasta database. Methionine oxidation, acetyl (Protein Nterm) was set as variable modification, and enzyme specificity was set to trypsin, allowing a maximum of one missed cleavage. A fragment-ion mass tolerance of 0.4 Da and a parent-ion tolerance of 10 ppm were set. Scaffold (Proteome Software Inc., version 5.2.2) was used to validate MS/MS-based peptide and protein identifications. Peptide identifications were accepted if they achieved a false discovery rate (FDR) of less than 0.1% by the Scaffold Local FDR algorithm. Protein identifications were accepted if they achieved an FDR of less than 1.0% and contained at least two identified peptides.

Supplementary Information The online version contains supplementary material available at https://doi.org/10.1007/s12217-024-10155-3.

Acknowledgements We thank the European Space Agency (ESA, SciSpacE) for providing access to the GraviTower Bremen Prototype. We also thank PRODEX (ESA), the Swiss Space Office (SSO), and Lucerne School of Engineering and Architecture (Switzerland) for their financial support. We thank Brigitte Herzog and Eva Hänsenberger from the University of Zurich (Switzerland), as well as the Center of Applied Space Technology and Microgravity (ZARM) for their support. We acknowledge the Func-tional Genomics Center Zurich (FGCZ) of University of Zurich and ETH Zurich, and in particular Sibylle Pfammatter, for the support on proteomics analyses.

Authors' Contribution S.L.W.: Conceptualization, Data curation, Funding acquisition, Investigation, Methodology, Software, Writing; G.C., J.P.: Investigation, Methodology; S.G., C.Z., L.R., R.E., B.B.: Methodology; C.J.: Software; J.T., M.H., D.I.P., K.F.R.: Investigation C.G.: Project administration; F.I., M.E.: Writing, Funding acquisition; G.S, S.S.L.: Methodology, Supervision, Funding acquisition.

Funding Open access funding provided by Lucerne University of Applied Sciences and Arts. This study was funded through PRODEX (ESA), the Swiss Space Office (SSO), the Lucerne School of Engineering and Architecture (Switzerland), and the University of Zurich (Switzerland). Access to the GraviTower Bremen Prototype was funded by the European Space Agency (ESA, SciSpacE). The funding bodies had no influence on the decision-making process, study design, or data interpretation.

Data Availability The data are available from the corresponding author upon reasonable request.

Declarations

Ethics Approval This set of animal experiments and procedures was performed in accordance with standard ethical guidelines, local laws, and restrictions and was approved by the Cantonal Veterinary Office of the Canton of Zurich.

Consent to Participate and to Publish Not applicable. No human subjects were involved in this study.

Competing Interests The authors declare no competing interests.

References

Alper, S.L.: Genetic Diseases of PIEZO1 and PIEZO2 Dysfunction. Curr. Top. Membr. **79**, 97–134 (2017). https://doi.org/10.1016/bs.ctm.2017.01.001

Anishkin, A., Loukin, S.H., Teng, J., Kung, C.: Feeling the hidden mechanical forces in lipid bilayer is an original sense. Proc. Natl. Acad. Sci. U.S.A. **111**(22), 7898–7905 (2014). https://doi.org/10.1073/pnas.1313364111

Arnadottir, J., Chalfie, M.: Eukaryotic mechanosensitive channels. Annu. Rev. Biophys. **39**, 111–137 (2010). https://doi.org/10.1146/annurev.biophys.37.032807.125836

Blaber, E., Marcal, H., Burns, B.P.: Bioastronautics: the influence of microgravity on astronaut health. Astrobiology **10**(5), 463–473 (2010). https://doi.org/10.1089/ast.2009.0415

Clément, G.: Fundamentals of space medicine. Space technology library, vol. 17. Springer, Dordrecht, NE (2007)

Coste, B., Mathur, J., Schmidt, M., Earley, T.J., Ranade, S., Petrus, M.J., Dubin, A.E., Patapoutian, A.: Piezo1 and Piezo2 are essential components of distinct mechanically activated cation channels. Science **330**(6000), 55–60 (2010). https://doi.org/10.1126/science.1193270

Dai, J., Sheetz, M.P.: Mechanical properties of neuronal growth cone membranes studied by tether formation with laser optical tweezers. Biophys. J . **68**(3), 988–996 (1995). https://doi.org/10.1016/S0006-3495(95)80274-2

Demontis, G.C., Germani, M.M., Caiani, E.G., Barravecchia, I., Passino, C., Angeloni, D.: Human Pathophysiological Adaptations to the Space Environment. Front. Physiol. **8**, 547 (2017). https://doi.org/10.3389/fphys.2017.00547

Dittus, H.: Drop tower 'bremen': A weightlessness laboratory on earth. Endeavour **15**(2), 72–78 (1991). https://doi.org/10.1016/S0160-9327(05)80008-0

Gierse, A., Kaczmarczik, U., Greif, A., Selig, H., von Kampen, P., Könemann, T., Lämmerzahl, C.: A Fast and Self-Acting Release-Caging-Mechanism for Actively Driven Drop Tower Systems. Microgravity Sci. Technol. **29**(5), 403–414 (2017). https://doi.org/10.1007/s12217-017-9560-y

Gierse, A., Könemann, T., von Kampen, P., Avilad, M.: The GraviTower Bremen Pro – Experiences with a next-generation drop tower system. Paper presented at the 73rd International Astronautical Congress (IAC), Paris, France, 2022

Gottlieb, P.A., Sachs, F.: Piezo1: properties of a cation selective mechanical channel. Channels (Austin) **6**(4), 214–219 (2012). https://doi.org/10.4161/chan.21050

Graf, J., Schulz, H., Wehland, M., Corydon, T.J., Sahana, J., Abdelfattah, F., Wuest, S.L., Egli, M., Krüger, M., Kraus, A., Wise, P.M., Infanger, M., Grimm, D.: Omics Studies of Tumor Cells under Microgravity Conditions. Int. J. Mol. Sci. **25**(2), 926 (2024)

Gu, Y., Gu, C.: Physiological and pathological functions of mechanosensitive ion channels. Mol. Neurobiol. **50**(2), 339–347 (2014). https://doi.org/10.1007/s12035-014-8654-4

Hughes, C.S., Foehr, S., Garfield, D.A., Furlong, E.E., Steinmetz, L.M., Krijgsveld, J.: Ultrasensitive proteome analysis using paramagnetic bead technology. Mol. Syst. Biol. **10**(10), 757 (2014). https://doi.org/10.15252/msb.20145625

Kohn, F.P.M., Ritzmann, R.: Gravity and neuronal adaptation, in vitro and in vivo-from neuronal cells up to neuromuscular responses: a first model. Eur. Biophys. J. (2017). https://doi.org/10.1007/s00249-017-1233-7

Könemann, T., Kaczmarczik, U., Gierse, A., Greif, A., Lutz, T., Mawn, S., Siemer, J., Eigenbrod, C., von Kampen, P., Lämmerzahl, C.: Concept for a next-generation drop tower system. Adv. Space Res. **55**(6), 1728–1733 (2015). https://doi.org/10.1016/j.asr.2014.12.028

Kufner, E., Blum, J., Callens, N., Eigenbrod, C., Koudelka, O., Orr, A., Rosa, C.C., Vedernikov, A., Will, S., Reimann, J., Wurm, G.: ESA's Drop Tower Utilisation Activities 2000 to 2011. Microgravity Sci. Technol. **23**(4), 409–425 (2011). https://doi.org/10.1007/s12217-011-9261-x

Lacroix, J.J., Botello-Smith, W.M., Luo, Y.: Probing the gating mechanism of the mechanosensitive channel Piezo1 with the small molecule Yoda1. Nat. Commun. **9**(1), 2029 (2018). https://doi.org/10.1038/s41467-018-04405-3

Lewis, A.H., Grandl, J.: Inactivation Kinetics and Mechanical Gating of Piezo1 Ion Channels Depend on Subdomains within the Cap. Cell Rep. **30**(3), 870-880.e872 (2020). https://doi.org/10.1016/j.celrep.2019.12.040

Lin, Y., Buyan, A., Corry, B.: Computational studies of Piezo1 yield insights into key lipid-protein interactions, channel activation, and agonist binding. Biophys. Rev. **14**(1), 209–219 (2022). https://doi.org/10.1007/s12551-021-00847-0

Richard, S., Henggeler, D., Ille, F., Vadrucci Beck, S., Moeckli, M., Forster, I.C., Franco-Obregón, A., Egli, M.: A Semi-automated Electrophysiology System for Recording from Xenopus Oocytes Under Microgravity Conditions. Microgravity Sci. Technol. **24**(4), 237–244 (2012). https://doi.org/10.1007/s12217-012-9307-8

Rocio Servin-Vences, M., Moroni, M., Lewin, G.R., Poole, K.: Direct measurement of TRPV4 and PIEZO1 activity reveals multiple mechanotransduction pathways in chondrocytes. eLife **6**, e21074 (2017). https://doi.org/10.7554/eLife.21074

Sachs, F.: Stretch-activated ion channels: what are they? Physiology (Bethesda) **25**(1), 50–56 (2010). https://doi.org/10.1152/physiol.00042.2009

Sachs, F., Morris, C.E.: Mechanosensitive ion channels in nonspecialized cells. Rev. Physiol. Biochem. Pharmacol. **132**, 1–77 (1998)

Schaffhauser, D.F., Andrini, O., Ghezzi, C., Forster, I.C., Franco-Obregon, A., Egli, M., Dittrich, P.S.: Microfluidic platform for electrophysiological studies on Xenopus laevisoocytes under varying gravity levels. Lab Chip **11**(20), 3471–3478 (2011). https://doi.org/10.1039/C0LC00729C

Soattin, L., Fiore, M., Gavazzo, P., Viti, F., Facci, P., Raiteri, R., Difato, F., Pusch, M., Vassalli, M.: The biophysics of piezo1 and piezo2 mechanosensitive channels. Biophys. Chem. **208**, 26–33 (2016). https://doi.org/10.1016/j.bpc.2015.06.013

Stühmer, W., Parekh, A.B.: Electrophysiological Recordings from Xenopus Oocytes. In: Sakmann, B., Neher, E. (eds.) Single-Channel Recording, pp. 341–356. Springer, US, Boston, MA (1995)

Syeda, R., Xu, J., Dubin, A.E., Coste, B., Mathur, J., Huynh, T., Matzen, J., Lao, J., Tully, D.C., Engels, I.H., Petrassi, H.M., Schumacher, A.M., Montal, M., Bandell, M., Patapoutian, A.: Chemical activation of the mechanotransduction channel Piezo1. Elife **4** (2015). https://doi.org/10.7554/eLife.07369

Türker, C., Akal, F., Joho, D., Panse, C., Barkow-Oesterreicher, S., Rehrauer, H., Schlapbach, R.: B-Fabric: the Swiss Army Knife for life sciences. Paper presented at the Proceedings of the 13th International Conference on Extending Database Technology, Lausanne, Switzerland, 2010

Wang, Y., Xiao, B.: The mechanosensitive Piezo1 channel: structural features and molecular bases underlying its ion permeation and mechanotransduction. J. Physiol. **596**(6), 969–978 (2018). https://doi.org/10.1113/JP274404

Wang, Y., Chi, S., Guo, H., Li, G., Wang, L., Zhao, Q., Rao, Y., Zu, L., He, W., Xiao, B.: A lever-like transduction pathway for long-distance chemical- and mechano-gating of the mechanosensitive Piezo1 channel. Nat. Commun. **9**(1), 1300 (2018). https://doi.org/10.1038/s41467-018-03570-9

Wijerathne, T.D., Ozkan, A.D., Lacroix, J.J.: Yoda1's energetic footprint on Piezo1 channels and its modulation by voltage and temperature. Proc. Natl. Acad. Sci. **119**(29), e2202269119 (2022). https://doi.org/10.1073/pnas.2202269119

Williams, D., Kuipers, A., Mukai, C., Thirsk, R.: Acclimation during space flight: effects on human physiology. CMAJ : Canadian Medical Association journal = journal de l'Association medicale canadienne **180**(13), 1317–1323 (2009). https://doi.org/10.1503/cmaj.090628

Wuest, S.L., Roesch, C., Ille, F., Egli, M.: Calcium dependent current recordings in Xenopus laevis oocytes in microgravity. Acta astronautica **141**(Supplement C), 228–236 (2017). https://doi.org/10.1016/j.actaastro.2017.10.003

Wuest, S.L., Gantenbein, B., Ille, F., Egli, M.: Electrophysiological experiments in microgravity: lessons learned and future challenges. NPJ Microgravity **4**, 7 (2018). https://doi.org/10.1038/s41526-018-0042-3

Zeng, W.Z., Marshall, K.L., Min, S., Daou, I., Chapleau, M.W., Abboud, F.M., Liberles, S.D., Patapoutian, A.: PIEZOs mediate neuronal sensing of blood pressure and the baroreceptor reflex. Science **362**(6413), 464–467 (2018). https://doi.org/10.1126/science.aau6324